Rapid Communication J. Biochem. 131, 313–317 (2002)

Crystal Structure of 1-Deoxy-D-xylulose 5-phosphate Reductoisomerase Complexed with Cofactors: Implications of a Flexible Loop Movement upon Substrate Binding[1]

Shunsuke Yajima,*[,2] Takamasa Nonaka,† Tomohisa Kuzuyama,‡ Haruo Seto,‡[,3] and Kanju Ohsawa*

Department of Bioscience, Tokyo University of Agriculture, Setagaya-ku, Tokyo 156-8502; †Department of BioEngineering, Nagaoka University of Technology, Nagaoka, Niigata 940-2188; and ‡Institute of Molecular and Cellular Biosciences, The University of Tokyo, Bunkyo-ku, Tokyo 113-0032

Received December 9, 2001; accepted January 10, 2002

The key enzyme in the nonmevalonate pathway, 1-deoxy-D-xylulose 5-phosphate reductoisomerase (DXR), has been shown to be an effective target of antimalarial drugs. Here we report the crystal structure of DXR complexed with NADPH and a sulfate ion from *Escherichia coli* at 2.2 Å resolution. The structure showed the presence of an extra domain, which is absent from other NADPH-dependent oxidoreductases, in addition to the conformation of catalytic residues and the substrate binding site. A flexible loop covering the substrate binding site plays an important role in the enzymatic reaction and the determination of substrate specificity.

Key words: crystal structure, *Escherichia coli*, MAD, nonmevalonate pathway, reductoisomerase.

In all living organisms, isoprenoids such as steroid hormones, carotenoids, and ubiquinone or menaquinone play important roles (*1*). From the initial discovery of the mevalonate pathway, it was widely accepted that isopentenyl diphosphate, the fundamental unit in terpenoid biosynthesis, was only formed through the mevalonate pathway. However, it has recently been shown that many organisms, including most eubacteria and green algae, and the chloroplasts of higher plants use the nonmevalonate pathway for the formation of isopentenyl diphosphate (*2*).

DXR is a key enzyme in the nonmevalonate pathway and catalyzes the intramolecular rearrangement accompanied by reduction of 1-deoxy-D-xylulose 5-phosphate (DXP) to give 2-*C*-methyl-D-erythritol 4-phosphate (MEP) (*3, 4*) (Fig. 1).

More recently, it was shown that the antibiotic fosmidomycin and its derivatives inhibited DXR from *Plasmodium falciparum*, and cured mice infected with the rodent malaria parasite *P. cinckei* (*5*). Malaria parasites lacking the mevalonate pathway use the nonmevalonate pathway associated with apicoplasts (*5*). Therefore, new efficient drugs for combating the disease are now being extensively pursued.

Since the nonmevalonate pathway is absent in mammals, inhibitors of the enzymes involved in the pathway are considered to be very promising antimalarial drugs. In order to screen large libraries of compounds or to conduct *de novo* design, structural information on target proteins can be very effective and we thus started to study the crystal structure of DXR from *Escherichia coli*.

The recombinant selenomethionyl DXR (*6*) was crystallized by the hanging drop vapor diffusion method. Each droplet consisted of equal volumes of a reservoir buffer containing 1.65 M ammonium sulfate and 0.06 M potassium sodium (+)-tartrate in 0.1 M sodium citrate buffer (pH 5.6), and a solution of 20 mg/ml protein in 20 mM TrisCl (pH 8.5), 10% glycerol, 100 mM KCl, 1 mM $MgCl_2$, 3 mM NADPH, and 1mM DTT. The crystals belong to space group $P2_12_12$ with cell parameters of a = 182.72 Å, b = 56.16 Å, c = 72.64 Å, and two monomers per asymmetric unit. Diffraction data was collected at SPring-8 BL41XU for Multiwavelength Anomalous Diffraction (MAD). The diffraction data were merged and scaled using the programs MOSFLM (*7*) and SCALA (*8*), and the data were solved using the program SOLVE (*9*). 34 out of 38 selenium sites were determined with SOLVE. An initial electron density map was modified using the program RESOLVE (*10*). Model building was performed with QUANTA (Molecular Simulations), and the data were refined at 100–2.2 Å with the program CNS (*11*). The collected data and refinement statistic are presented in Table I. Because of the His-tagged construct, recombinant DXR had 398 residues with extra sequences of 9 and 16 at the N-terminal and C-terminal, respectively. However, no apparent electron density was observed for these extra residues except one and two at the N and C-terminals, respectively. The quality of the refined model was analyzed with the program PROCHEK (*8*), 99.5% of the total residues being in most favoured regions (92.9%) or additional allowed regions (6.6%), and 0.5% in generously

[1] This work was supported in part by the High-Tech Research Center of Tokyo University of Agriculture (S.Y.).

[2] To whom correspondence should be addressed. E-mail: yshun@nodai.ac.jp

[3] Present address: Department of Applied Biology and Chemistry, Tokyo University of Agriculture, Setagaya-ku, Tokyo 156-8502.

Abbreviations: DX, 1-deoxyxylulose; DXR, 1-deoxy-D-xylulose 5-phosphate reductoisomerase; MEP, 2-*C*-methyl-D-erythritol 4-phosphate; MAD, multiplewavelength anomalous diffraction.

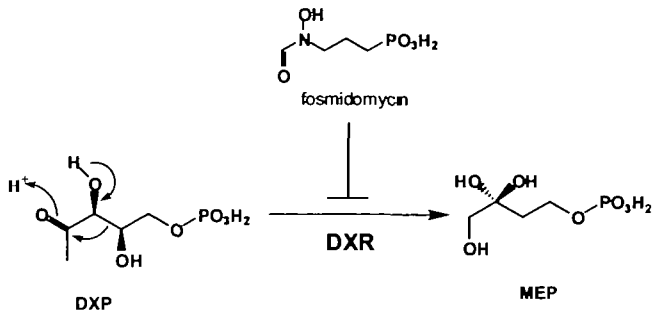

Fig. 1. **DXR reaction.** DXR catalyzes the conversion of 1-deoxy-D-xylulose 5-phosphate (DXP) to 2-*C*-methyl-D-erythritol 4-phosphate (MEP).

TABLE I. **Data collection and refinement statistics.**

Data collection			
Wavelength (Å)	0.983971	0.979311	0.979155
	Remote	Edge	Peak
Resolution (Å)	2.2	2.2	2.2
Observed reflections	312,434	310,525	308,135
Unique reflections	47,895	48,168	48,260
Completeness (%)[a]	98.8 (90.8)	99.0 (91.7)	99.0 (91.5)
R_{sym}[a,b]	0.065 (0.315)	0.079 (0.379)	0.093 (0.468)
I/σ[a]	10.2 (2.3)	8.2 (1.9)	7.0 (1.6)
Refinement statistics			
R_{work}/R_{free}[c]	0.213/0.240		
R.m.s.d from ideal geometry			
Bonds (Å)	0.006		
Angles (°)	1.2		

[a]Values in parentheses are for the highest resolution shell. [b]$R_{sym} = \Sigma|I_h - \langle I_h \rangle|/\Sigma I_h$ over all h, where I_h is the intensity of reflection h. [c]A subset of the data (10%) was excluded from the refinement and used to calculate R_{free}.

allowed regions in the Ramachandran plot. Since the crystals for native DXR did not give good diffraction data, we proceeded to use the selenomethionyl protein alone for this study.

The structure was obtained as a homodimer conformation in an asymmetric unit (Fig. 2a). The monomer structure is composed of three domains: an N-terminal NADPH binding domain (blue in Fig. 2b), a central domain (orange), and a C-terminal α-helical domain (green). The NADPH binding domain exhibits an α/β topology with a seven-stranded parallel β-sheet and 7 α-helices, which is as canonical as the NAD(P)H-binding fold. The central domain contains a four-stranded β-sheet and 7 helices consisting of a 2-layer sandwich fold. β strand 8 (β8), β10, and β11 comprise an antiparallel, and β8 and β9 are in a parallel conformation. One side of the β-sheet constitutes the protein surface, and the other side faces inside of the protein to form a pocket interfaced with parts of the N-terminal and C-terminal domains. A structural homology search of this domain with DALI (*12*) and CE (*13*) revealed the catalytic domains of several oxidoreductases such as glyceraldehyde 3-phosphate dehydrogenase (GAPDH) (*14*) and dihydrodipicolinate reductase (*15*). The topologies of β-sheets were identical among DXR and these enzymes, while they have longer β-strands than DXR does, and GAPDH has a longer loop with strands and helices between strands corresponding to β10 and β11 of DXR.

The C-terminal α-helical domain hosted long four helices. The central domain and C-terminal domain are connected by a long loop (colored yellow in Fig. 2) spanning over the central domain, and the loop contributes as the interface of a monomer-monomer interaction. The dimer interface also constituted an eight-stranded β-sheet arranged side by side in the central domains (Fig. 2a).

NAD(P)H-dependent oxidoreductases usually hold two domain structures with NAD(P)H domains and catalytic domains. Although DXR can also be categorized into this class and shows structural similarity in the corresponding domains with some oxidoreductases, the overall DXR structure is rather unique due to the presence of the additional third domain.

We previously conducted mutational analysis of DXR to demonstrate that the four amino acid residues His153, His209, Glu231, and His257 are responsible for the enzyme catalysis (*16*). The present crystal structural studies show that all these residues are located in the central domain (Fig. 2b) with their side chains protruding into the pocket (Fig. 3a). Therefore, we conclude that this pocket formed by the central domain and parts of the N-terminal and C-terminal domains indeed acts as the catalytic pocket.

Since DXR requires NADPH and divalent cations for its activity (*6*), we added the coenzyme and Mg^{2+} to the protein solution for crystallization. We also tried to obtain a complex of DXR with the inhibitor fosmidomycin (*17*). After extensive screening, we were only able to obtain a crystal complexed with NADPH, *i.e.* not one with Mg^{2+} or fosmidomycin. In addition to NADPH, a sulfate ion was trapped in the catalytic pocket. Since fosmidomycin molecule possesses the phosphonate function, and the substrate DXP possesses the phosphate function, it is highly possible that the position of the sulfate ion in the crystal represents where the phosphonate or phosphate function is located in the DXR protein.

The sulfate ion is fixed through a hydrogen bond with one of the catalytic residues, His209 (Fig. 3a). The mutation of His209 to Gln caused a drastic decrease of the wild-type k_{cat}/K_m value to 5,200-fold (*16*). Interestingly, inspection of the structure revealed that there is no site of entry into the catalytic pocket for substrates and that the loop portion between His209 through Met214 showed higher B-factor values than other parts, the average values being 40 for all residues and 105 for the loop region (Fig. 3a). This suggests that this loop may act as a "hatch" that closes the active site when the substrate has entered the catalytic pocket. The hydrogen bond between His209 and the phosphate function could close the hatch to fix the substrate effectively. The fixation of the phosphate function of a substrate seems to be very important for the activity. When 1-deoxyxylulose (DX) lacking a phosphate function was used as the substrate in place of DXP, the oxidation of NADPH was not observed (*16*). This implies that the fixation of the phosphate function is necessary to anchor the substrate at the correct position or to latch the hatch loop to close the pocket. Besides the hydrogen bond through His209, this loop provides hydrophobic conditions with Trp212 and Met214 (Fig. 3b). This would be preferable for DXR to interact with the hydrophobic backbone of a substrate such as DXP or fosmidomycin.

The mutation of His153 to Gln did not change the k_{cat}/K_m value so much as the other three residues did. This may be explained by that the structure with His153 is surrounded

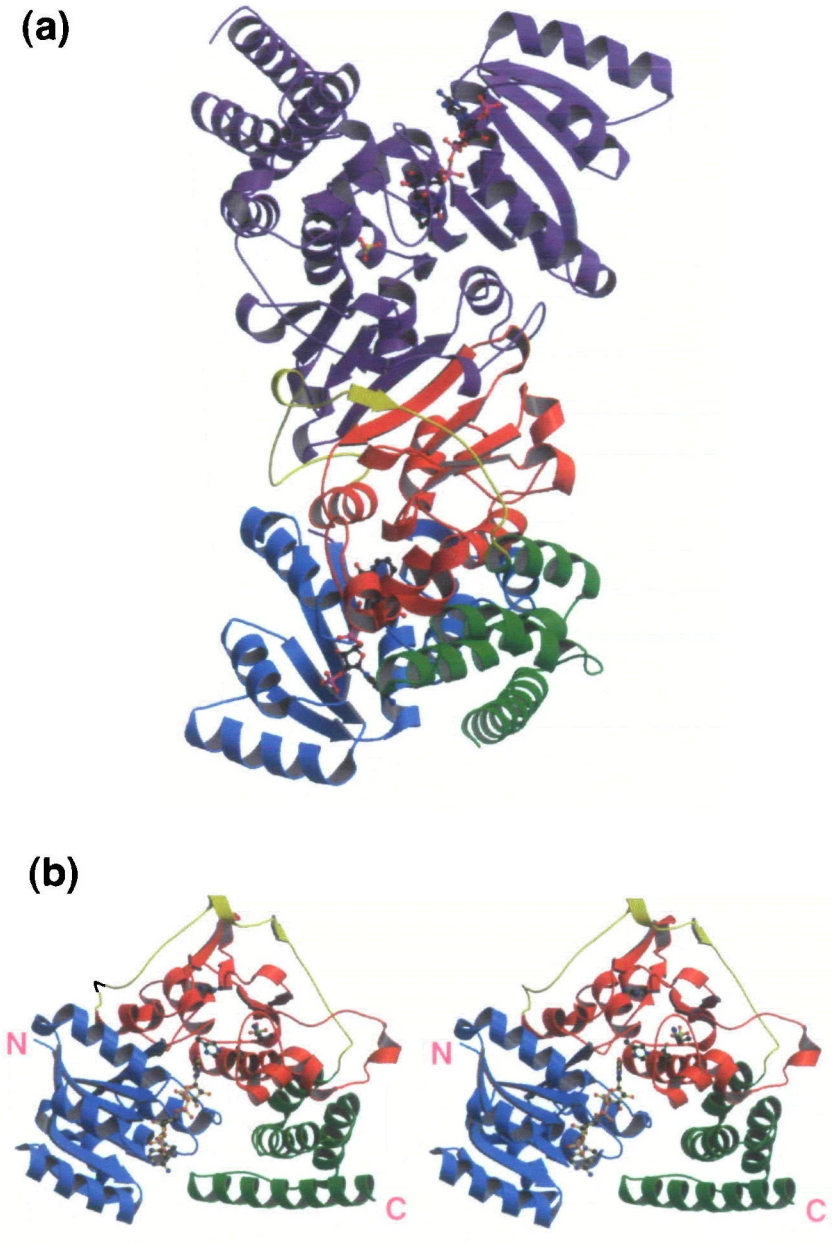

Fig. 2. **Overall structure of DXR.** (a) Ribbon diagram of the homodimer. One monomer is colored purple, and the other is colored blue, orange, and green for each domain. NADPH and a sulfate ion are shown as ball-and-stick models. (b) Stereo view of the monomer. The NADPH-domain, catalytic domain, and C-terminal domain are colored blue, orange, and green, respectively. The connecting loop between the catalytic domain and the C-terminal domain is colored yellow. Four catalytic residues, H153, H209, E231, and H257, NADPH and a sulfate ion are shown as ball-and-stick models, and colored in green for catalytic residues, and yellow for both NADPH and the ion. Figures 2 and 3 were prepared with MOLSCRIPT (*25*) and RASTER3D (*26*).

by Asp150, Glu152, and Glu231 (Fig. 3a), making direct contact with substrates difficult. Therefore, His153 may mainly have a structural role rather than act in the catalysis. A mutational change of His257, the fourth catalytic residue, decreased the k_{cat}/K_m value most drastically, *i.e.* by 27,000-fold. Moreover, only this mutation changed the K_m value as to NADPH, despite the fact that it is located farther from NADPH in the catalytic pocket. This mutation may affect the structure of the catalytic pocket or the solvent environment in the pocket by disrupting the hydrogen bond network. It remains, however, unknown how His257 can work as one of the catalytic residues.

Glu231 proved to be the most important residue for the catalysis (*16*) because the mutation of Glu231 to Lys only changed its k_{cat} value, *i.e.* not K_m. The function of Glu231 may be explained by the analogy with acetohydroxy acid isomeroreductase from spinach (PDB code: 1YVE) (*18*). This enzyme requires divalent cations, DXR as does. In the catalytic pocket of this plant enzyme, one aspartic acid and three glutamic acid residues hold two magnesium ions. These ions are octahedrally coordinated by water molecules and a substrate in addition to these acidic residues. One of the cations plays a role in the isomerization step and the other is needed for the reduction step (*18, 19*). Although no Mg^{2+} was found in the DXR structure in this study, this enzyme also hosts one aspartic acid and three glutamic acid residues in the catalytic pocket. It is difficult to predict the octahedral coordination for Mg^{2+} since no substrates bind to the catalytic pocket. These acidic residues, Asp150, Glu152, Glu231, and Glu234, however, are positioned approximately around 3 to 4 Å apart from O^{δ} or O^{ε} of each residue (Fig. 3a), and are conserved among DXRs from various species. Therefore, it is highly likely that these acidic residues harbor divalent cations and are necessary to con-

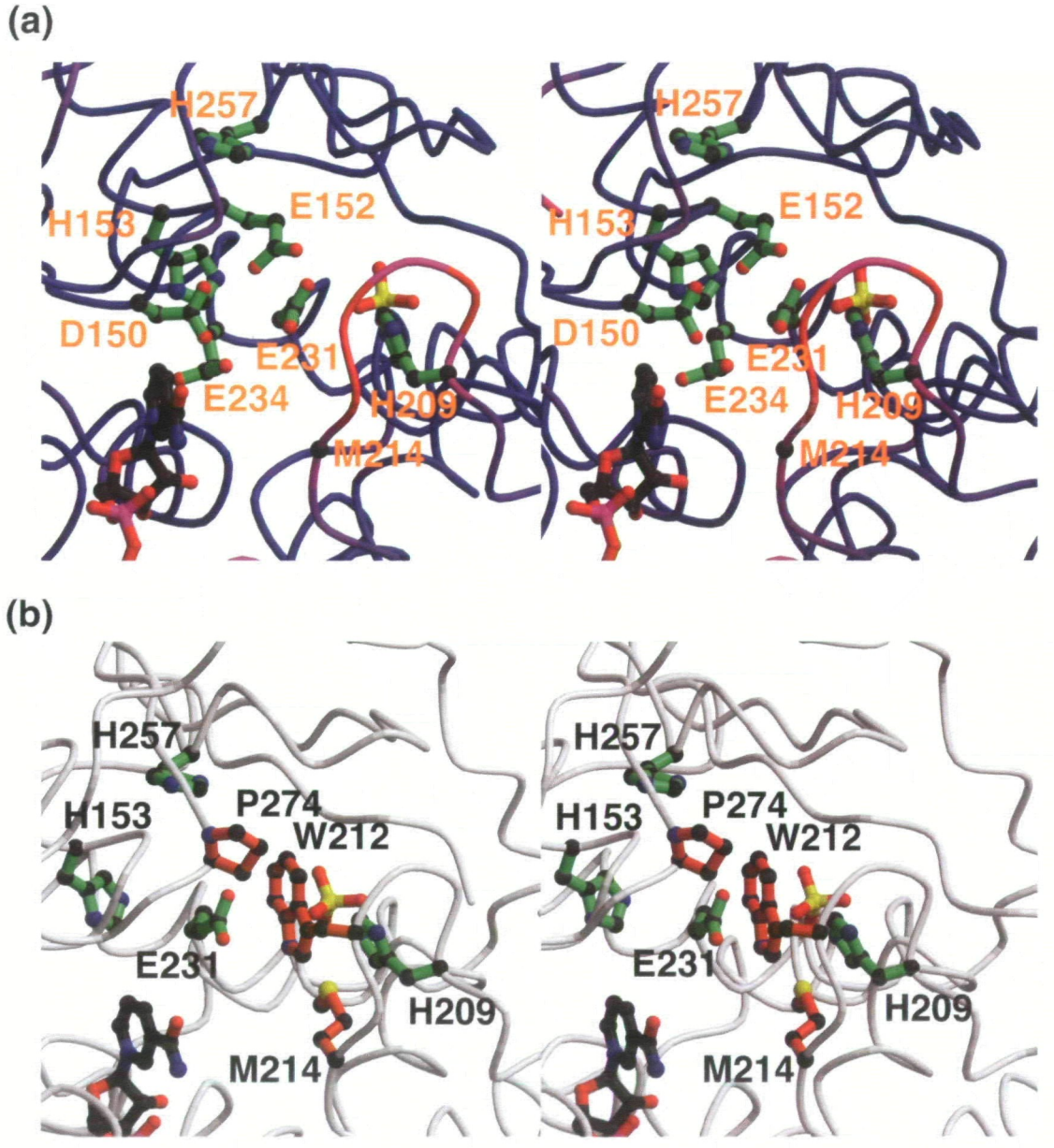

Fig. 3. **Stereo representations of the catalytic pocket of DXR.** (a) The previously detected four catalytic residues (H153, H209, E231, and H257) and other acidic residues (D150, E152, and E234), which are potentially responsible for metal ion binding in the catalytic pocket, are shown in yellow-green. The peptide backbone is colored with a gradient of blue to red according to the B-factor value. Only the loop part (residues 209 to 214) has a high B-factor value (red). The Cα position of M214 is presented for clarification. (b) Four catalytic residues are colored green and three hydrophobic residues in the catalytic pocket are colored orange. These hydrophobic ones are expected to interact with the substrate backbone.

fer activity to DXR.

DXR uses NADPH as a cofactor but not NADH. When it was replaced with NADH, the activity decreased to about 1% of the original level (*20*). Judging from the DXR structure determined in this study, Thr10 anchors the 2′ phosphate function of NADPH through a hydrogen bond, and Lys37 may fix the phosphate residue through electrostatic interaction (*21*). NADH lacking the phosphate function may fail to establish these interactions necessary for activity. Interestingly, this Thr10 residue is conserved in all DXRs from nine species detailed below, implying the importance of this residue in NADPH binding. DXR belongs to the class B dehydrogenases because it uses the pro-*S* hydrogen at the 4 position of the nicotinamide ring (*22, 23*). Our structure supports this result in that the pro-*S* hydrogen extends towards the catalytic pocket whereas the pro-*R* hydrogen protrudes out of the pocket. Very recently, the crystal structure of DXR from *E. coli* without NADPH and other cofactors has been reported, the space group being $C222_1$ with three monomers per asymmetric unit (PDB code: 1K5H) (*24*). In their structure, the three monomers show different domain conformations, suggesting the domain mobility of DXR. On the other hand, in our structure, the domain conformations are fixed. In conjunction with

the flexible loop described above, the binding of cofactors and the ligand would cause significant mobility for an induced fit of the enzyme. For better understanding of the catalytic mechanism of DXR, we are continuing to try to crystallize a complex of DXR with fosmidomycin.

Atomic coordinates have been deposited in the Protein Data Bank (accession code 1JVS).

We wish to thank Dr. M. Kawamoto for the assistance at BL41XU, SPring-8.

REFERENCES

1. Sacchettini, J.C. and Poulter, C.D. (1997) Creating isoprenoid diversity. *Science* **277**, 1788–1789
2. Rohmer, M. (1999) *Comprehensive Natural Products Chemistry*, Vol. 2, pp. 45–67, Elsevier, Amsterdam
3. Duvold, T., Bravo, J.M., Pale-Grosdemange, C., and Rohmer, M. (1997) Biosynthesis of 2-*C*-methyl-D-erythritol, a putative C-5 intermediate in the mevalonate independent pathway for isoprenoid biosynthesis. *Tetrahedron Lett.* **38**, 4769–4772
4. Duvold, T., Cali, P., Bravo, J.M., and Rohmer, M. (1997) Incorporation of 2-*C*-methyl-D-erythritol, a putative isoprenoid precursor in the mevalonate-independent pathway, into ubiquinone and menaquinone of *Escherichia coli*. *Tetrahedron Lett.* **38**, 6181–6184
5. Jomaa, H. *et al.* (1999) Inhibitors of the nonmevalonate pathway of isoprenoid biosynthesis as antimalarial drugs. *Science* **285**, 1573–1576
6. Takahashi, S., Kuzuyama, T., Watanabe, H., and Seto, H. (1998) A 1-deoxy-D-xylulose 5-phosphate reductoisomerase catalyzing the formation of 2-*C*-methyl-D-erythritol 4-phosphate in an alternative nonmevalonate pathway for terpenoid biosynthesis. *Proc. Natl. Acad. Sci. USA* **95**, 9879–9884
7. Leslie, A.G.W. (1992) Recent changes to the MOSFLM package for processing film and image plate data. *Joint CCP4+ESF-EAMCB Newsletter on Protein Crystallography*, No. 26
8. Collaborative Computational Project, Number 4 (1994) The CCP4 suite: programs for protein crystallography. *Acta Crystallogr. D* **50**, 760–763
9. Terwilliger, T.C. and Berendzen, J. (1999) Automated MAD and MIR structure solution. *Acta Crystallogr. D* **55**, 849–861
10. Terwilliger, T.C. (2000) Maximum likelihood density modification. *Acta Crystallogr. D* **56**, 965–972
11. Brünger, A.T. *et al.* (1998) Crystallography and NMR system: a new software suite for macromolecular structure determination. *Acta Crystallogr. D* **54**, 905–921
12. Holm, L. and Sander, C. (1993) Dali programme. *J. Mol. Biol.* **233**, 123–138
13. Shindyalov, I.N. and Bourne, P.E. (1998) Protein structure alignment by incremental combinatorial extension (CE) of the optimal path. *Protein Eng.* **11**, 739–747
14. Yun, M., Park, C-G., Kim, J-Y., and Park, H-W. (2000) Structural analysis of glyceraldehyde 3-phosphate dehydrogenase from *Escherichia coli:* direct evidence of substrate binding and cofactor-induced conformational changes. *Biochemistry* **39**, 10702–10710
15. Scapin, G., Reddy, S.G., Zheng, R., and Blanchard, J.S. (1997) Three-dimensional structure of *Escherichia coli* dihydrodipicolinate reductase in complex with NADH and the inhibitor 2,6-pyridinedicarboxylate. *Biochemistry* **36**, 15081–15088
16. Kuzuyama, T., Takahashi, S., Takagi, M., and Seto, H. (2000) Characterization of 1-deoxy-D-xylulose 5-phosphate reductoisomerase, an enzyme involved in isopentenyl diphosphate biosynthesis, and identification of its catalytic amino acid residues. *J. Biol. Chem.* **275**, 19928–19932
17. Kuzuyama, T., Shimizu, T., Takahasi, S., and Seto, H. (1998) Fosmidomycin, a specific inhibitor of 1-deoxy-D-xylulose 5-phosphate reductoisomerase in the nonmevalonate pathway for terpenoid biosynthesis. *Tetrahedron Lett.* **39**, 7913–7916
18. Biou, V. *et al.* (1997) The crystal structure of plant acetohydroxy acid isomeroreductase complexed with NADPH, two magnesium ions and a herbicidal transition state analog determined at 1.65 Å resolution. *EMBO J.* **16**, 3405–3415
19. Dumas, R., Butikofer, M-C., Job, D., and Douce, R. (1995) Evidence for two catalytically different magnesium-binding sites in acetohydroxy acid isomeroreductase by site-directed mutagenesis. *Biochemistry* **34**, 6026–6036
20. Kuzuyama, T., Takahashi, S., Watanabe, H., and Seto, H. (1998) Direct formation of 2-C-methyl-D-erythritol 4-phosphate from 1-deoxy-D-xylulose 5-phosphate by 1-deoxy-D-xylulose in the non-mevalonate pathway to isopentenyl diphosphate. *Tetrahedron Lett.* **39**, 4509–4512
21. Tanaka, N., Nonaka, T., Nakamura, K., and Hara, A. (2000) SDR: structure, mechanism of action, and substrate recognition. *Curr. Org. Chem.* **4**, 945–957
22. Proteau, P.J., Woo, Y.H., Williamson, R.T., and Phaosiri, C. (1999) Stereochemistry of the reduction step mediated by 1-deoxy-D-xylulose 5-phosphate isomeroreductase. *Org. Lett.* **1**, 921–923
23. Radykewicz, T. *et al.* (2000) Biosynthesis of terpenoids: 1-deoxy-D-xylulose 5-phosphate reductoisomerase from *Escherichia coli* is a class B dehydrogenase. *FEBS Lett.* **465**, 157–160
24. Reuter, K., Sanderbrand, S., Jomaa, H., Wiesner, J., Steinbrecher, I., Beck, E., Hintz, M., Klebe, G., and Stubbs, M.T. (2002) Crystal structure of 1-deoxy-D-xylulose-5-phosphate reductoisomerase, a crucial enzyme in the non-mevalonate pathway of isoprenoid biosynthesis. *J. Biol. Chem.* **277**, 5378–5384
25. Kraulis, P.J. (1991) MOLSCRIPT: a program to produce both detailed and schematic plots of protein structures. *J. Appl. Crystallogr.* **24**, 946–950
26. Merritt, E.A. and Murphy, M.E.P. (1994) Raster3D version 2.0. A program for photorealistic molecular graphics. *Acta Crystallogr. D* **50**, 869–873